

Short Papers

The Dynamic Capability Equations: A New Tool for Analyzing Robotic Manipulator Performance

Alan Bowling and Oussama Khatib

Abstract—Dynamic capability equations (DCE) provide a new description of robot acceleration and force capabilities. These refer to a manipulator's ability to accelerate its end-effector and to apply forces to the environment at the end-effector. The key features in the development of these equations are that they combine the analysis of end-effector accelerations, velocities, and forces, while addressing the difference in units between translational and rotational quantities. The equations describe the magnitudes of translational and rotational acceleration and force guaranteed to be achievable in every direction, from a particular configuration, given the limitations on the manipulator's motor torques. They also describe the effect of velocities on these capabilities contributed by the Coriolis and centrifugal forces, as well as the reduction of actuator torque capacity due to motor speed. This article focuses on nonredundant manipulators with as many actuators as degrees of freedom.

Index Terms—Acceleration, dynamic performance, dynamics, end-effector, force, manipulator, robotics.

I. INTRODUCTION

The purpose of the proposed performance analysis is to provide tools to aid in the design and control of robots. The aspects of manipulator performance considered here are the *acceleration and force*¹ *capabilities*. They describe a robotic manipulator's ability to accelerate its end-effector, and to apply forces to the environment at the end-effector, given its actuator torque limitations. These capabilities determine a mechanism's capacity for manipulating grasped and nongrasped objects, and comprise what is referred to as *dynamic performance* or *dynamic manipulability*. The discussion in this paper is focused on nonredundant robotic manipulators which have as many actuators as degrees of freedom (DOFs), although this method can apply to other types of manipulators. The three main contributions of the proposed analysis concern the following:

- 1) unification of acceleration, velocity, and force analysis;
- 2) treatment of translational and rotational properties;
- 3) description of worst-case dynamic capabilities.

Unification of Performance Analyses: The proposed unification provides a common framework for characterizing the tradeoffs between a manipulator's different capabilities. In contrast, almost all

Manuscript received January 1, 2004; revised May 22, 2004. This paper was recommended for publication by Associate Editor S. Ma and Editor I. Walker upon evaluation of the reviewers' comments. This paper was presented in part at the 10th CISM-IFTOMM Symposium on Theory and Practice of Robots and Manipulators, Gdansk, Poland, September 1995, in part at the IEEE/RSJ International Conference on Intelligent Robots and Systems, Pittsburgh, PA, August 1995, and in part at the IEEE/RSJ International Conference on Intelligent Robots and Systems, Victoria, BC, Canada, October 1998.

A. Bowling is with the Robotics and Dynamic Systems Laboratory, Department of Aerospace and Mechanical Engineering, University of Notre Dame, Notre Dame, IN 46556 USA (e-mail: abowling@nd.edu).

O. Khatib is with the Robotics Laboratory, Department of Computer Science, Stanford University, Stanford, CA 94305 USA (e-mail: khatib@cs.stanford.edu).

Digital Object Identifier 10.1109/TRO.2004.837243

¹In this paper, the term "force" is meant to refer to forces and moments, unless otherwise indicated.

studies of manipulator performance isolate acceleration, velocity, and force in their analysis. These quantities are related to actuator torques in the equations of motion, and thus can be combined into one performance analysis by considering their equivalent actuator torques. The torque requirements for each quantity are compared against the available torque in order to determine the extent of the manipulator's capabilities; see Section III. The motivation for combining these analyses stems from the fact that many tasks involve simultaneously applying forces while sustaining motion. For instance, consider the task of polishing the surface of a cylinder or manipulating an object by pushing or pulling it. It is also desirable to include a velocity analysis, since the robot may be in motion while performing these tasks.

Treatment of Unit Inhomogeneity: Few studies of the acceleration and force capabilities have addressed the difference in units between translational and rotational motions and forces, which creates difficulties for many performance analyses. A number of studies raise concerns about the validity of analyses which do not adequately address the unit-inhomogeneity issue, including [1]–[4]. The *dynamic capability equations* (DCE) discussed herein were developed to treat this issue. The approach followed here is to map representations of translational and rotational quantities with different units into representations of actuator torques with the same units so that they can be compared, similar to what is done in the unification discussed above. As evidenced in [1]–[4], the unit-inhomogeneity issue can complicate a performance analysis, and thus, a careful treatment is required in order to obtain useful results. This is discussed further in Section IV.

Worst-Case Dynamic Performance: The proposed analysis also provides a description of the worst-case combinations of a manipulator's dynamic capabilities. The worst case is examined, because it provides a lower bound on the manipulator's capabilities, which allows for a concise summary of the system's performance. This is discussed further in Section II. This approach yields a description of the magnitudes of end-effector acceleration and force that the mechanism is *guaranteed* to be capable of producing in or about any direction, given the limitations on its actuator torque capacities. Worst-case velocities are also considered, whose impact is felt through the centrifugal and Coriolis forces, and the decrease in actuator torque capacity with motor speed described by the speed-torque curve [5]. The remainder of this paper presents a detailed development of the DCE, along with an example of their use in evaluating the dynamic performance of robotic manipulators.

II. BACKGROUND

The prior works most closely related to the proposed analysis consider dynamic effects on performance, which include the inertial properties and the limitations or bounds on the amount of torque the actuators can produce. The *inertial properties*, as perceived at the end-effector, describe the resistance to acceleration experienced by a force acting at the end-effector [6]–[10]. In contrast, the proposed study and others like it investigate the actuator effort required to accelerate the end-effector. These analyses explore the mapping between *end-effector acceleration space* and *actuator torque space*, obtained from the equations of motion, using different representations of available torque and attainable acceleration. Fig. 1 illustrates the various representations used in these studies, and highlights their differences for a 2-DOF planar manipulator example.

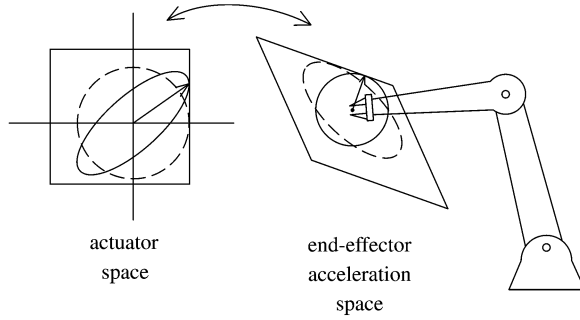


Fig. 1. Analysis of manipulator performance.

The bounds on actuator torque capacity, or *torque bounds*, are represented by the rectangle in actuator space shown in Fig. 1. These bounds are mapped into end-effector acceleration space yielding the *acceleration parallelepiped* [11] or *polytope* shown at the end-effector of the manipulator.

The vector within the parallelepiped shows one possible translational acceleration of the *operational point*, which is represented by the small circle at the end-effector. Any such acceleration vector that can be drawn within the parallelepiped is attainable. The parallelepiped's shape indicates an imbalance in acceleration capability, in that larger accelerations are achievable in some directions than in others.

Another approach shown in Fig. 1 involves the dashed circle in actuator space, which is mapped into the dashed ellipse in the end-effector acceleration space, yielding the *dynamic manipulability ellipsoid* [12], [13]. The solid circle in the end-effector acceleration space represents the *isotropic acceleration* that is mapped into the solid ellipse in actuator space, used in this paper and in [11], [12], [14], and [15].

The radius of the solid circle in Fig. 1 is referred to as the *balanced translational acceleration* and is similar to the *acceleration radius* in [14]; however, the acceleration radius applies to a range of configurations. It represents the *largest translational acceleration which is guaranteed to be achievable in every direction*. This measure is used because it is obtained by mapping accelerations into actuator torques, which facilitates the unification of performance analyses and treatment of unit inhomogeneities discussed herein.

The vector within the parallelepiped in Fig. 1 is the *worst-case translational acceleration*, which represents the magnitude and direction of the smallest acceleration of the operational point that can be achieved. The torque bound in contact with the ellipse indicates the *limiting actuator*, which saturates attempting to provide the worst-case acceleration. The *worst-case translational acceleration direction*, limiting actuator, and balanced translational acceleration, exemplify the key results from the proposed analysis.

Herein, additional *balanced quantities* will be examined: the *balanced acceleration*, *balanced force*, and *balanced velocity*. The balanced acceleration refers to either or both of the *balanced translational and rotational accelerations*, and likewise for the other terms. The spirit of this terminology also applies to references to acceleration, force, or velocity not explicitly modified by the terms “translational” and “rotational.” In this paper, forces and velocities are considered within the context of dynamic performance. However, these quantities are usually investigated from a kinematic viewpoint; kinematic velocity studies include the *manipulability ellipsoid* [16] and velocity polytope [17], and kinematic force studies include the force ellipsoid and polytope, found in [18] and [19], respectively.

Most analyses examine only one of acceleration, velocity, or force, with the exception of [6] and [15], which considered accelerations and velocities together. However, these studies did not directly address the

unit-inhomogeneity issue, and neither do most studies. Exceptions include a kinematic study in [20] which eliminates the rotational velocities by referencing the Jacobian to the translational velocities of multiple reference points on the end-effector. Scaling factors were used in the kinematic studies [21], [22]; however, they can be somewhat arbitrary and may not adequately address the problem [2]. Translational and rotational velocities were separated for the special case of manipulators with spherical wrists in [23]. A more general separation of translational and rotational quantities is used herein, in [7] for the inertial properties, and in [24] for velocity polytopes.

III. UNIFICATION OF PERFORMANCE ANALYSIS

The mappings of accelerations, velocities, and forces into actuator torques are defined by the equations of motion

$$E \begin{bmatrix} \dot{\mathbf{v}} \\ \dot{\boldsymbol{\omega}} \end{bmatrix} + \mathcal{E} \begin{bmatrix} \mathbf{f} \\ \mathbf{m} \end{bmatrix} + \mathbf{C}(\mathbf{v}, \boldsymbol{\omega}) + \mathbf{g} = \boldsymbol{\Upsilon} \quad (1)$$

where $\mathbf{v} \in \mathbb{R}^r$ and $\boldsymbol{\omega} \in \mathbb{R}^p$ are the end-effector translational and rotational velocities, and $\dot{\mathbf{v}} \in \mathbb{R}^r$ and $\dot{\boldsymbol{\omega}} \in \mathbb{R}^p$ are the associated end-effector accelerations with respect to an inertial reference frame. $\mathbf{f} \in \mathbb{R}^r$ and $\mathbf{m} \in \mathbb{R}^p$ are the end-effector contact forces and moments. $E \in \mathbb{R}^{n \times n}$, $\mathcal{E} \in \mathbb{R}^{n \times n}$, $\mathbf{g} \in \mathbb{R}^n$, $\boldsymbol{\Upsilon} \in \mathbb{R}^n$, and $\mathbf{C}(\mathbf{v}, \boldsymbol{\omega}) \in \mathbb{R}^n$ are the inertia matrix, force transmission matrix, gravity forces, actuator torques, and the Coriolis and centrifugal forces and other velocity-dependent terms. The robot is assumed to have n DOF and $n = r + p$. Equation (1) is developed in detail in Appendix I.

The development of (1) depends on the existence of an invertible *actuator Jacobian*, $J_a \in \mathbb{R}^{n \times n}$, expressed as

$$\begin{bmatrix} \mathbf{v} \\ \boldsymbol{\omega} \end{bmatrix} = J_a \dot{\boldsymbol{\theta}} \quad (2)$$

where $\dot{\boldsymbol{\theta}} \in \mathbb{R}^n$ are the motor speeds. Thus systems with a nonsquare or singular actuator Jacobian cannot directly apply the analysis as presented herein. Redundant, underactuated, overactuated, or redundantly actuated manipulators have a nonsquare actuator Jacobian. Generalized inverses are usually employed in this situation; however, each one will yield a different description of manipulator capabilities, and it is usually unclear which to choose. A more complete description can be obtained by augmenting the actuator Jacobian, adding or subtracting rows, in order to obtain a square matrix. Singularities can be similarly handled. Much work on redundant manipulators has been done [25] and will be published later; examination of the other cases is ongoing.

A common problem in analyses dependent on the Jacobian or actuator Jacobian mapping in (2) is that the results are *point-specific*. The translational velocity \mathbf{v} in either Jacobian is referenced to a specific operational point on the end-effector, and the rotational velocity $\boldsymbol{\omega}$ represents end-effector rotations about that point. However, different operational points yield different results which may not be equivalent. These results are *not invariant to translation or relocation of the operational point*. It is difficult to satisfy this type of invariance and still obtain a physically meaningful description of the manipulator capabilities, as suggested in [3].

Equation (1) and the torque bounds include all of the elements considered in the performance analyses discussed in Section II, except for the bounds on joint velocities. However, these limits can be incorporated into the model, currently in a limited way, because they are related to the torque bounds through the motor speed as described by the speed-torque curve. Here, it is assumed that the torque bounds can be modeled using a polynomial function of rotor angular velocity $\dot{\theta}_i$

$$\Upsilon_{\text{bound}_i} = \Upsilon_{\text{peak}_i} + k_i(\dot{\theta}_i) \quad (3)$$

where Υ_{peak_i} is the constant peak/maximum torque of the i th actuator, and $k_i(\dot{\theta}_i)$ is a polynomial excepting the constant term Υ_{peak_i} . Equation (3) can be linear or nonlinear.

Currently, the speed-torque curve must be approximated using only the quadratic term in $k_i(\dot{\theta}_i)$ for compatibility with the centrifugal and Coriolis forces. Otherwise, only a purely numerical approach can be used to explore the velocity effects. An operating region can be chosen where torque capacity is approximately independent of rotor velocity, $k_i(\dot{\theta}_i) = 0$, eliminating the modeling issues; the velocity limits should then be included as additional constraints in this analysis. Υ_{peak_i} can also be chosen by the user. Equation (3) can be expressed as

$$-\Upsilon_{\text{peak}} \leq \Upsilon + \mathbf{k} \quad \Upsilon - \mathbf{k} \leq \Upsilon_{\text{peak}} \quad (4)$$

which must be satisfied independently, or row by row, as must all inequalities developed hereafter; $\Upsilon_{\text{peak}} \in \mathbb{R}^n$ and $\mathbf{k} \in \mathbb{R}^n$.

IV. UNIT INHOMOGENEITY

It becomes difficult to assign a physical interpretation to the representations in Fig. 1 when both translational and rotational quantities are involved. The polytope and ellipsoid mix translational and rotational accelerations, making it difficult to draw conclusions about either. The ellipsoid approach yields physically inconsistent results when units are mixed [1], as does the balanced-acceleration approach.

When translational and rotational quantities are mixed, the results are not invariant to changes in units, which means that a simple scaling of units can produce different results which are not equivalent to each other. As suggested in [1], three aspects of invariance can be considered for a performance analysis: invariance to changes in units, to rotations of the Euclidean coordinates, and to translation of the origin/operational point. The DCE satisfy the first two, but not the third, as discussed in Section III.

The approach followed here is to separate translational and rotational quantities. Thus the equations of motion (1), combined with the torque bounds in (4), are expressed as

$$\begin{aligned} \Upsilon_{\text{upper}} &\geq E_v \dot{\mathbf{v}} + E_\omega \dot{\boldsymbol{\omega}} + \mathcal{E}_f \mathbf{f} + \mathcal{E}_m \mathbf{m} + \bar{\mathbf{h}} \\ \Upsilon_{\text{lower}} &\leq E_v \dot{\mathbf{v}} + E_\omega \dot{\boldsymbol{\omega}} + \mathcal{E}_f \mathbf{f} + \mathcal{E}_m \mathbf{m} + \underline{\mathbf{h}} \end{aligned} \quad (5)$$

where

$$\begin{aligned} E &= [E_v \quad E_\omega] \quad \mathcal{E} = [\mathcal{E}_f \quad \mathcal{E}_m] \\ \Upsilon_{\text{upper}} &= \Upsilon_{\text{peak}} - \mathbf{g} \quad \bar{\mathbf{h}} = \mathbf{C}(\mathbf{v}, \boldsymbol{\omega}) - \mathbf{k} \\ \Upsilon_{\text{lower}} &= -\Upsilon_{\text{peak}} - \mathbf{g} \quad \underline{\mathbf{h}} = \mathbf{C}(\mathbf{v}, \boldsymbol{\omega}) + \mathbf{k}. \end{aligned} \quad (6)$$

The terms that are constant at a given configuration are collected in the bounds Υ_{upper} and Υ_{lower} . As stated earlier, the unit-inhomogeneity issue is addressed by mapping separate representations of quantities with different units, into actuator torques having the same units. This process is discussed next.

V. ANALYSIS OF DYNAMIC PERFORMANCE

A. Overview

The proposed analysis involves specifying the manipulator configuration, acceleration, velocity, and force in the equations of motion (1), in order to determine the actuator torques required to produce the latter quantities. The results are then compared against the available torque, as described by the torque bounds in (4), in order to determine the extent of the specified motions and forces; this comparison is expressed in (5). Separate balanced quantities are used to specify all quantities which have homogeneous units

$$\begin{aligned} \dot{\mathbf{v}}^T \dot{\mathbf{v}} &= |\dot{v}|^2 & \dot{\boldsymbol{\omega}}^T \dot{\boldsymbol{\omega}} &= |\dot{\omega}|^2 \\ \mathbf{f}^T \mathbf{f} &= |\mathbf{f}|^2 & \mathbf{m}^T \mathbf{m} &= |\mathbf{m}|^2 \\ \mathbf{v}^T \mathbf{v} &= |v|^2 & \boldsymbol{\omega}^T \boldsymbol{\omega} &= |\omega|^2. \end{aligned} \quad (7)$$

$|\dot{v}|$ is the balanced translational acceleration, a positive scalar which constrains the magnitude of the acceleration vector $\|\dot{\mathbf{v}}\|$, and likewise

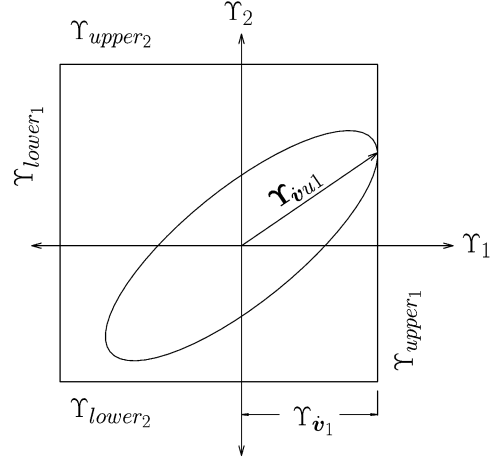


Fig. 2. Torque vector component in direction of $\Upsilon_{\text{upper}_1}$.

for the other balanced quantities. *In general, each relation in (7) represents a sphere of radius $|\cdot|$.*

Each inequality in (5) is considered independently, thus each term in a single relation can be maximized or minimized, for the upper and lower bounds respectively, subject to the constraints in (7), to determine the worst-case contribution from that term. These worst-case contributions can be summed for each relation, yielding a set of inequalities describing the extent of the balanced quantities. The terms in a single inequality all have the same units, so there is no unit problem.

This process sounds simple, yet it may not be intuitively obvious why it would yield a correct result. The geometric argument presented in the next sections examines the mappings of balanced quantities into actuator torques, and in doing so, justifies the proposed process and provides insights into the character of the problem and its solution. It also illustrates the unification of performance analyses and treatment of unit inhomogeneity resulting in the DCE.

Representing each term in (5) as an actuator torque facilitates the discussion of the geometric argument

$$\Upsilon_{\text{upper}} \geq \Upsilon_{\dot{\mathbf{v}}} + \Upsilon_{\dot{\boldsymbol{\omega}}} + \Upsilon_{\mathbf{f}} + \Upsilon_{\mathbf{m}} + \Upsilon_{\bar{\mathbf{h}}} \triangleq \bar{\Upsilon} \quad (8)$$

$$\Upsilon_{\text{lower}} \leq \Upsilon_{\dot{\mathbf{v}}} + \Upsilon_{\dot{\boldsymbol{\omega}}} + \Upsilon_{\mathbf{f}} + \Upsilon_{\mathbf{m}} + \Upsilon_{\underline{\mathbf{h}}} \triangleq \underline{\Upsilon} \quad (9)$$

where $\Upsilon_{\dot{\mathbf{v}}} = E_v \dot{\mathbf{v}}$, and likewise for the other terms, excepting $\Upsilon_{\bar{\mathbf{h}}} = \bar{\mathbf{h}}$ and $\Upsilon_{\underline{\mathbf{h}}} = \underline{\mathbf{h}}$.

B. Geometric Argument: A Simple Example

The geometric argument is best understood using a simple example, such as the 2-DOF manipulator shown in Fig. 1, assuming that only the $\Upsilon_{\dot{\mathbf{v}}}$ term in (8) and (9) is nonzero

$$\Upsilon_{\text{upper}} \geq \Upsilon_{\dot{\mathbf{v}}} \triangleq \bar{\Upsilon} \quad \Upsilon_{\text{lower}} \leq \Upsilon_{\dot{\mathbf{v}}} \triangleq \underline{\Upsilon}. \quad (10)$$

This geometric argument involves visualizing the terms in (10) as geometric objects, and exploring the relationships between them. As discussed in Section II, the bounds Υ_{upper} and Υ_{lower} can be represented by a rectangle in actuator space, as shown in Fig. 2 for the 2-DOF planar manipulator. Fig. 2 also shows the torque ellipse obtained by mapping an acceleration circle into actuator space, as described in

$$\dot{\mathbf{v}}^T \dot{\mathbf{v}} = |\dot{v}|^2 \xrightarrow{E_v \dot{\mathbf{v}} = \Upsilon_{\dot{\mathbf{v}}}} \Upsilon_{\dot{\mathbf{v}}}^T \left(E_v E_v^T \right)^{-1} \Upsilon_{\dot{\mathbf{v}}} = |\dot{v}|^2. \quad (11)$$

When the torque ellipse is inscribed within the bounds, as shown in Fig. 2, no larger balanced translational acceleration is attainable. The proposed analysis is based on exploring the conditions under which this occurs. This is accomplished by examining the vector $\Upsilon_{\dot{v}u1}$ in Fig. 2, representing the contact point between the torque ellipse and upper bound on Υ_1 .

Of the vectors comprising the torque ellipse, $\Upsilon_{\dot{v}_{u1}}$ is the one with the largest component $\Upsilon_{\dot{v}_1}$ in the direction of the bound that it touches, $\Upsilon_{\text{upper}_1}$. Thus the value of the $\Upsilon_{\dot{v}_1}$ component of vector $\Upsilon_{\dot{v}_{u1}}$ is unique in the set of values for $\Upsilon_{\dot{v}_1}$ from each vector comprising the torque ellipse. Due to this uniqueness, maximizing the general form of $\Upsilon_{\dot{v}_1}$ subject to (7) yields its extreme value $(\Upsilon_{\dot{v}_1})_{\text{max}}$ as well as $\Upsilon_{\dot{v}_{u1}}$.

In order to determine the actual numerical value of $(\Upsilon_{\dot{v}_1})_{\text{max}}$, the size of the ellipse must be known *a priori*. Since this is not known, the component is maximized considering the balanced acceleration $|\dot{v}|$ as a parameter, *not a decision variable*, in the optimization; note that the result must then be expressed in terms of this parameter. Thus, the maximization yields the form of the extreme value, rather than the actual numerical value of the extremum. This result is compared against the known numerical value of the bound to determine the actual size of the balanced translational acceleration $|\dot{v}|$.

The maximum value of the $\Upsilon_{\dot{v}_1}$ component, $(\Upsilon_{\dot{v}_1})_{\text{max}}$, is unique and can be found in terms of $|\dot{v}|$ as

$$\begin{aligned} \max_{\dot{v}} \Upsilon_{\dot{v}_1} &:= E_{v_1} \dot{v} \\ \text{subject to } \dot{v}^T \dot{v} &= |\dot{v}|^2 \end{aligned} \quad (12)$$

where E_{v_i} is the i th row of E_v . This problem has a closed-form solution, \dot{v}_{u1} , the *worst-case translational acceleration*, which is found using Lagrange multipliers

$$\dot{v}_{u1} = |\dot{v}| \hat{v}_{u1} = |\dot{v}| \frac{E_{v_1}^T}{\|E_{v_1}\|} \quad \Upsilon_{\dot{v}_{u1}} = E_v \dot{v}_{u1} \quad (13)$$

where \hat{v}_{u1} is a unit vector in the worst-case translational acceleration direction with respect to the $\Upsilon_{\text{upper}_1}$ boundary. The details of this solution are given in Appendix II.

When the optimal value $(\Upsilon_{\dot{v}_1})_{\text{max}}$ equals $\Upsilon_{\text{upper}_1}$, the torque ellipse touches the bounds; however, this condition is expressed as in (14) so that all boundaries can be checked

$$(\Upsilon_{\dot{v}_1})_{\text{max}} = E_{v_1} \dot{v}_{u1} = \|E_{v_1}\| |\dot{v}| \leq \Upsilon_{\text{upper}_1}. \quad (14)$$

Since the torque ellipse touches the bound $\Upsilon_{\text{upper}_1}$, the corresponding actuator Υ_1 is the limiting actuator for the example in Fig. 2. Usually the limiting actuator is not known beforehand, so all boundaries must be checked. This involves checking the points where the torque ellipse would be tangent to each boundary, by maximizing and minimizing each torque vector component. A torque ellipse within the bounds satisfies

$$\begin{bmatrix} (\Upsilon_{\dot{v}_1})_{\text{max}} \\ (\Upsilon_{\dot{v}_2})_{\text{max}} \\ -(\Upsilon_{\dot{v}_1})_{\text{min}} \\ -(\Upsilon_{\dot{v}_2})_{\text{min}} \end{bmatrix} = \begin{bmatrix} \|E_{v_1}\| |\dot{v}| \\ \|E_{v_2}\| |\dot{v}| \\ \|E_{v_1}\| |\dot{v}| \\ \|E_{v_2}\| |\dot{v}| \end{bmatrix} \leq \begin{bmatrix} \Upsilon_{\text{upper}} \\ -\Upsilon_{\text{lower}} \end{bmatrix}. \quad (15)$$

All of the above solutions are unique. The extent of the balanced translational acceleration is determined by the largest value of $|\dot{v}|$ satisfying all of the relations in (15).

Notice that the examination of each torque vector component corresponds to considering the inequalities in (10) row by row, which justifies the statement after (4). $(\Upsilon_{\dot{v}_i})_{\text{max}}$ and $(\Upsilon_{\dot{v}_i})_{\text{min}}$ are the worst-case contributions of the $\Upsilon_{\dot{v}}$ term to the inequalities corresponding to $\Upsilon_{\text{upper}_i}$ and $\Upsilon_{\text{lower}_i}$ in (10), respectively, which are used to obtain the inequalities in (15), as discussed in Section V-A.

C. Geometric Argument: Addressing Unit Inhomogeneity

The results from Section V-B do not directly apply to manipulators whose end-effector motions are described in terms of translations and rotations. The overall procedure does apply. Consider the case where only accelerations are involved

$$\Upsilon_{\text{upper}} \geq \Upsilon_{\dot{v}} + \Upsilon_{\dot{\omega}} = \bar{\Upsilon} \quad \Upsilon_{\text{lower}} \leq \Upsilon_{\dot{v}} + \Upsilon_{\dot{\omega}} = \underline{\Upsilon} \quad (16)$$

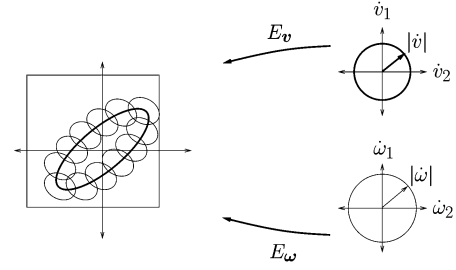


Fig. 3. Torque ellipse addition.

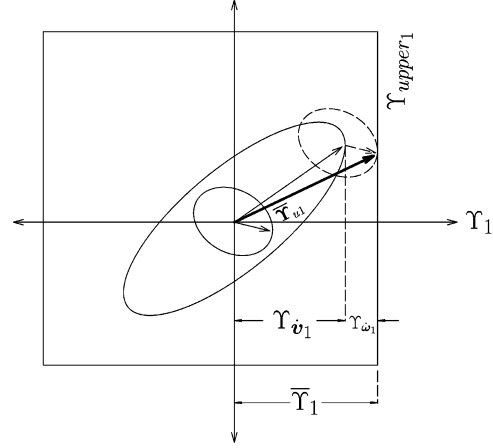


Fig. 4. Translational and rotational acceleration torque components.

obtained from (8) and (9). Due to the increased dimension of the actuator motion space, the bounds Υ_{upper} and Υ_{lower} are visualized geometrically as a *right-angled hyperparallelepiped*. Keeping translations and rotations separate results in two torque ellipsoids, defined as

$$\dot{v}^T \dot{v} = |\dot{v}|^2 \xrightarrow[\dot{v} = E_v^+ \Upsilon_v]{\Upsilon_v^T (E_v^+)^T E_v^+ \Upsilon_v} |\dot{v}|^2 \quad (17)$$

$$\dot{\omega}^T \dot{\omega} = |\dot{\omega}|^2 \xrightarrow[\dot{\omega} = E_\omega^+ \Upsilon_\omega]{\Upsilon_\omega^T (E_\omega^+)^T E_\omega^+ \Upsilon_\omega} |\dot{\omega}|^2 \quad (18)$$

where the superscript “+” indicates the Moore–Penrose pseudoinverse, or left inverse, $E_v^+ = (E_v^T E_v)^{-1} E_v^T$. These mappings are valid, because both acceleration vectors are of smaller dimension than the actuator torque vector. The original relationship, $E_v \dot{v} = \Upsilon_v$ for instance, between the n torque vector components and the lower number of acceleration vector components, is defined by n relations, yielding an overconstrained system. Thus, there exists a one-to-one mapping between Υ_v and \dot{v} , and between Υ_ω and $\dot{\omega}$, which can be represented by the pseudoinverse. In general, the mappings in (17) and (18) yield ellipsoids in actuator space.

The addition of torques in (16) can be represented geometrically by mapping one torque ellipsoid onto every point on the surface of the other. This addition results in what is referred to as a *torque hypersurface*, which is difficult to visualize when it exists in a highly dimensional space. Fig. 3 gives a representation of the torque hypersurface which is technically inaccurate, yet adequately illustrates the concept.

The bold vector in Fig. 4, denoted Υ_{u1} , represents the contact point between the torque hypersurface and boundary $\Upsilon_{\text{upper}_1}$ shown in Fig. 3. The dashed ellipse is used to indicate where the torque hypersurface touches the bound. The composition of Υ_{u1} is shown in Fig. 4. The contribution of each torque ellipse to Υ_{u1} corresponds to the location where each would independently touch the boundary $\Upsilon_{\text{upper}_1}$. Thus, $(\bar{\Upsilon}_1)_{\text{max}} = (\Upsilon_{\dot{v}_1})_{\text{max}} + (\Upsilon_{\dot{\omega}_1})_{\text{max}}$, which is unique because $(\Upsilon_{\dot{v}_1})_{\text{max}}$ and $(\Upsilon_{\dot{\omega}_1})_{\text{max}}$ are unique, as are all such extreme

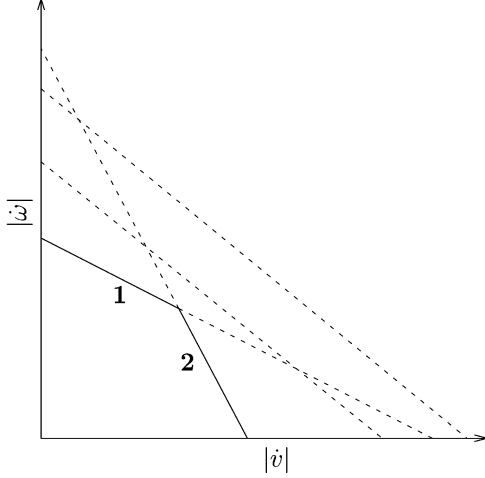


Fig. 5. Dynamic capability curve.

values. The uniqueness of $(\bar{\Upsilon}_1)_{\max}$ implies that $\bar{\Upsilon}_{u1}$ is also unique, which means the torque hypersurface touches each boundary at only one point. The form of the extreme values for each torque vector component can be found as

$$\begin{aligned} \max_{\dot{v}, \dot{\omega}} \text{ or } \min_{\dot{v}, \dot{\omega}} \bar{\Upsilon}_i &:= \Upsilon_{\dot{v}_i} + \Upsilon_{\dot{\omega}_i} = E_{v_i} \dot{v}_i + E_{\omega_i} \dot{\omega}_i \\ \text{subject to } \dot{v}^T \dot{v} &= |\dot{v}|^2 \quad \dot{\omega}^T \dot{\omega} = |\dot{\omega}|^2. \end{aligned} \quad (19)$$

Using Lagrange multipliers yields closed-form solutions to the problems in (19), which are the worst-case accelerations for each boundary \dot{v}_{ui} and $\dot{\omega}_{ui}$; see Appendix II. In the solution process, the terms involving translational and rotational acceleration completely decouple, eliminating the need to separately consider the optimization problems. These optimizations correspond to independently determining the worst-case contributions of the $\Upsilon_{\dot{v}}$ and $\Upsilon_{\dot{\omega}}$ terms in each relation of (16), in order to obtain the inequalities in (20), as discussed in Section V-A.

A torque hypersurface lying within the bounds must satisfy

$$\begin{bmatrix} \|E_{v_1}\| |\dot{v}| + \|E_{\omega_1}\| |\dot{\omega}| \\ \vdots \\ \|E_{v_n}\| |\dot{v}| + \|E_{\omega_n}\| |\dot{\omega}| \\ \|E_{v_1}\| |\dot{v}| + \|E_{\omega_1}\| |\dot{\omega}| \\ \vdots \\ \|E_{v_n}\| |\dot{v}| + \|E_{\omega_n}\| |\dot{\omega}| \end{bmatrix} \leq \begin{bmatrix} \Upsilon_{\text{upper}} \\ -\Upsilon_{\text{lower}} \end{bmatrix}. \quad (20)$$

The extent of the balanced translational and rotational accelerations and limiting actuator(s) are determined by the largest values of $|\dot{v}|$ and $|\dot{\omega}|$ which satisfy all of the relations in (20). However, note that this does not result in a single solution for $|\dot{v}|$ or $|\dot{\omega}|$, as occurred in Section V-B. The result is a curve which defines a relationship between $|\dot{v}|$ and $|\dot{\omega}|$.

This curve is found by overlaying on the same plot in the $|\dot{v}|-|\dot{\omega}|$ space the lines defined by each relation in (20). The lines forming the innermost envelope around the origin, shown as solid lines in Fig. 5, yield what is referred to as a *dynamic capability curve*, which is always *convex and piecewise linear*. The completely dashed lines represent two of the other inequalities in (20). The infinity of solutions for the balanced accelerations on and beneath this curve are achievable. Discontinuities appear when the torque hypersurface for different solutions touch different boundaries; Figs. 3 and 4 illustrate one possible solution. The numeric labels in Fig. 5 indicate the limiting actuators for the solutions along a segment of the curve.

D. Geometric Argument: Unification of Performance Analyses

This section focuses on adding considerations of force and velocity to the investigation of acceleration capability discussed in Section V-C, in order to unify the performance analyses of these quantities. Because the acceleration and force terms are linear with respect to the accelerations and forces, the treatment of acceleration in Section V-C can easily be extended to include the force terms in (8) and (9)

$$\begin{aligned} \Upsilon_{\text{upper}} &\geq \Upsilon_{\dot{v}} + \Upsilon_{\dot{\omega}} + \Upsilon_f + \Upsilon_m + \Upsilon_{\bar{h}} \triangleq \bar{\Upsilon} \\ \Upsilon_{\text{lower}} &\leq \Upsilon_{\dot{v}} + \Upsilon_{\dot{\omega}} + \Upsilon_f + \Upsilon_m + \Upsilon_{\underline{h}} \triangleq \underline{\Upsilon} \end{aligned}$$

yielding similar results with similar properties.

The difficulties occur when adding the velocity terms to the analysis. These problems are due to the nonlinearities in the velocity terms and the separation of translational and rotational velocities required to address the unit inhomogeneities. Nonlinearities are evident in the velocity terms expressed as

$$\Upsilon_{\bar{h}} = \bar{h} = \begin{bmatrix} \begin{bmatrix} v \\ \omega \end{bmatrix}^T \bar{H}_1 \begin{bmatrix} v \\ \omega \end{bmatrix} \\ \vdots \\ \begin{bmatrix} v \\ \omega \end{bmatrix}^T \bar{H}_n \begin{bmatrix} v \\ \omega \end{bmatrix} \end{bmatrix} \quad (21)$$

and likewise for $\Upsilon_{\underline{h}} = \underline{h}$. The $\bar{H}_i \in \mathbb{R}^{n \times n}$ in (21) are symmetric matrices containing the coefficients of each quadratic form. v and ω cannot be separated in (21) in order to obtain a simple mapping of velocity spheres into actuator torques. However, the image in actuator space of the spheres representing balanced velocities must be a bounded geometric object, because the velocities are represented by bounded, closed surfaces. Although difficult to visualize, this object can be used to form a torque hypersurface. Thus, it is still valid to consider where the torque hypersurface will touch the bounds, which leads to torque vector-component optimizations, just as in Sections V-B and V-C.

Because the velocity terms are purely quadratic, recalling the discussion of the speed-torque curve, there are always at least two solutions associated with the extreme value of each torque vector component. For instance, the extreme value $(\Upsilon_{\bar{h}_i})_{\max}$ is obtained from at least two solutions

$$\begin{aligned} (\mathbf{v}_{ui}, \boldsymbol{\omega}_{ui}) &= \{(\mathbf{v}_{ui1}, \boldsymbol{\omega}_{ui1}), (\mathbf{v}_{ui2}, \boldsymbol{\omega}_{ui2}) \dots\} \\ &= \{(\mathbf{v}_{ui1}, \boldsymbol{\omega}_{ui1}), (-\mathbf{v}_{ui1}, -\boldsymbol{\omega}_{ui1}) \dots\}. \end{aligned} \quad (22)$$

This means that the unit vectors in the worst-case velocity directions, $\hat{\mathbf{v}}_{ui}$ and $\hat{\boldsymbol{\omega}}_{ui}$, are not unique; the torque hypersurface may touch a particular boundary at more than one point. Yet, all solutions yield the same extreme value.

The component optimizations are expressed as

$$\begin{aligned} \max_{\dot{v}, \dot{\omega}, \mathbf{f}, \mathbf{m}, \mathbf{v}, \boldsymbol{\omega}} \bar{\Upsilon}_i \quad \text{or} \quad \min_{\dot{v}, \dot{\omega}, \mathbf{f}, \mathbf{m}, \mathbf{v}, \boldsymbol{\omega}} \underline{\Upsilon}_i \\ \text{subject to } \dot{v}^T \dot{v} &= |\dot{v}|^2 \quad \dot{\omega}^T \dot{\omega} = |\dot{\omega}|^2 \\ \mathbf{f}^T \mathbf{f} &= |\mathbf{f}|^2 \quad \mathbf{m}^T \mathbf{m} = |\mathbf{m}|^2 \\ \mathbf{v}^T \mathbf{v} &= |\mathbf{v}|^2 \quad \boldsymbol{\omega}^T \boldsymbol{\omega} = |\boldsymbol{\omega}|^2. \end{aligned} \quad (23)$$

These problems are nonconvex because of the nonlinear equality constraints [26]. When using Lagrange multipliers, the acceleration, force, and velocity terms decouple, allowing closed-form solutions for the acceleration and force terms, but not for the velocity terms. It is unlikely that a closed-form solution of an optimization with a nonlinear cost function and nonlinear constraints can be found [26].

Still, some analysis of the velocity terms is desired without resorting to a purely numerical solution. A numerical solution involves, for example, specifying a numerical value for $|v|$ and solving for the largest numerical value of $|\omega|$, yielding a single point as the solution.

The chosen approach is to add a constraint to (23)

$$|\omega| = \eta |v| \quad (24)$$

where a specific numerical value is assigned to the positive scalar η . Varying η from zero to ∞ yields the entire solution set. This is akin to changing variables, specifying only one of the new variables, and using the resulting equation to define the second. Although seemingly numerical, each η value yields an optimal value describing an infinity of solutions, such as

$$(\Upsilon_{\bar{h}_i})_{\max} = \begin{cases} \bar{c}_i |v|^2, & \eta < \infty \\ \bar{c}_i |\omega|^2, & \eta \rightarrow \infty \end{cases} \quad (25)$$

where \bar{c}_i is a scalar. This solution is given in Appendix III. This approach is used in a design methodology briefly discussed in Section VI.

Note that if a specific value is assigned to $|v|$, as in a purely numerical approach, a closed-form solution such as (25) cannot be found, in general. Only the corresponding numerical value of $|\omega|$ can be found using a numerical approach. A linear velocity term in the cost function of (23), as can be contributed by a linear approximation of the speed-torque curve, also requires a numerical approach. The constraint in (24) does not help this case. When the translational and rotational velocity subspaces are decoupled, a closed-form solution can be found. The decoupled cases include $\eta = 0$ and $\eta \rightarrow \infty$, or $|w = 0|$ and $|v = 0|$, respectively.

E. Dynamic Capability Equations

A torque hypersurface involving velocity effects for a particular value of η which lies within the bounds must satisfy

$$\mathbf{A} \begin{bmatrix} |v| \\ |\dot{\omega}| \end{bmatrix} + \mathbf{F} \begin{bmatrix} |f| \\ |m| \end{bmatrix} + \mathbf{C}(|v|^2, |\omega|^2) \leq \mathbf{T} \quad (26)$$

where

$$\mathbf{T} = \begin{bmatrix} \Upsilon_{\text{upper}}^T & -\Upsilon_{\text{lower}}^T \end{bmatrix}^T. \quad (27)$$

$\mathbf{A} \in \mathbb{R}^{2n \times 2}$ and $\mathbf{F} \in \mathbb{R}^{2n \times 2}$ are defined as

$$\begin{aligned} \mathbf{A}_i &= [\|E_{v_i}\| \quad \|E_{\omega_i}\|] \\ \mathbf{F}_i &= [\|E_{f_i}\| \quad \|E_{m_i}\|] \end{aligned} \quad (28)$$

and \mathbf{A}_i is the i th row of \mathbf{A} , and likewise for \mathbf{F} . The vector $\mathbf{C}(|v|^2, |\omega|^2) \in \mathbb{R}^{2n}$ is defined as

$$\mathbf{C}_i = \left(\Upsilon_{\bar{h}_i} \right)_{\max} \quad \mathbf{C}_{i+n} = - \left(\Upsilon_{\bar{h}_i} \right)_{\min}. \quad (29)$$

The relations in (26) are referred to as the DCE. The extent of the balanced quantities is determined by their largest values which satisfy (26). Just as in Section V-C, these equations describe relationships between the balanced quantities. These relationships are explored next.

F. Dynamic Capability Hypersurface

Each relation in the DCE can represent a hypersurface in a six-dimensional space due to the six unknown balanced quantities. If the hypersurfaces are overlaid in the same space, the ones forming the innermost envelope around the origin, referred to as the *dynamic capability hypersurface*, determine the extent of the balanced quantities. Since the hypersurface cannot be displayed, sections of it are examined in order to explore its properties. Fig. 6 shows a section where $|f| = |m| = |\omega| = \eta = 0$ for the PUMA 560 manipulator, at the configuration shown in Fig. 7. Note that the constraint in (24) yields a section of the hypersurface.

The limiting actuator is at the second joint, as indicated by the numeric label on the surface of Fig. 6. The worst-case directions are shown by the line segments emanating from the operational point of

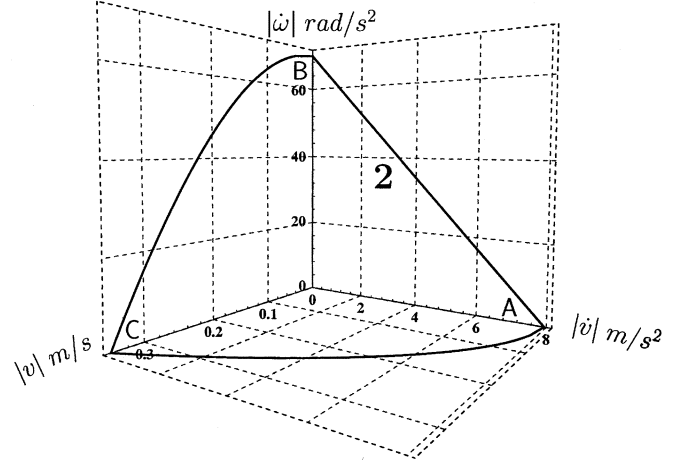


Fig. 6. PUMA 560 dynamic capability surface. This is a section of the dynamic capability hypersurface obtained using $|f| = |m| = |\omega| = \eta = 0$.

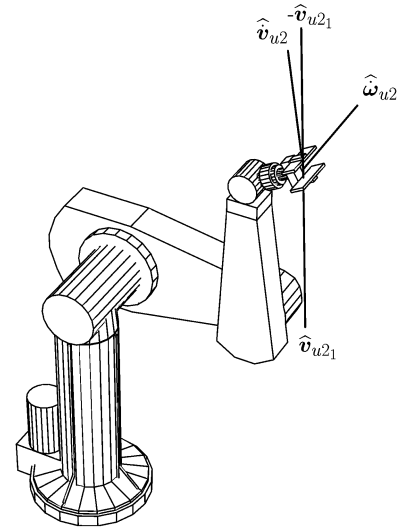


Fig. 7. PUMA 560 worst-case motion directions.

the PUMA 560 in Fig. 7. The PUMA 560 model used to obtain Fig. 6 is given in [27].

The curve in the $|\dot{v}||\dot{\omega}|$ plane of Fig. 6 is a dynamic capability curve similar to Fig. 5. Point **A** represents the intercept on the $|\dot{v}|$ axis, 7.9 m/s², which is the extent of balanced translational acceleration achievable from rest, if the end-effector does not rotate. Fig. 7 shows the worst-case direction of translational acceleration, \hat{v}_{u2} . The worst-case translational acceleration of the operational point from this configuration, associated with point **A**, is expressed as

$$\dot{v}_{u2} = |\dot{v}| \hat{v}_{u2} = (7.9 \text{ m/s}^2) \hat{v}_{u2}. \quad (30)$$

An equal or higher level of translational acceleration can be achieved in every direction other than \hat{v}_{u2} . The manufacturers of the PUMA 560 claim that it should be able to achieve 9.81 m/s² acceleration at the end-effector, so this result is reasonable. Note that \hat{v}_{u2} remains the same for all combinations of acceleration and velocity described by the surface in Fig. 6. However, the magnitude of the worst-case acceleration $|\dot{v}|$ decreases along the surface as velocity and angular acceleration increase.

Point **B** represents the intercept on the $|\dot{\omega}|$ axis, 70 rad/s², which is the extent of balanced rotational acceleration achievable from rest, if the end-effector operational point does not translate. Fig. 7 shows the

worst-case direction of rotational acceleration, $\hat{\omega}_{u_2}$. The worst-case angular acceleration of the end-effector about the operational point from this configuration, associated with point **B**, is expressed as

$$\dot{\omega}_{u_2} = |\dot{\omega}| \hat{\omega}_{u_2} = (70 \text{ rad/s}^2) \hat{\omega}_{u_2}. \quad (31)$$

$\dot{\omega}_{u_2}$ has properties similar to \dot{v}_{u_2} . The worst-case direction $\hat{\omega}_{u_2}$ remains the same for all combinations of acceleration and velocity described by the surface in Fig. 6. However, the magnitude of the worst-case angular acceleration, $|\dot{\omega}|$, decreases as velocity and translational acceleration increase.

The remainder of the surface describes the translational velocity effects on acceleration capability. The shape of the surface indicates that the balanced accelerations decrease to zero as the balanced translational velocity increases. Point **C** in Fig. 6 represents the magnitude of translational velocity, 0.34 m/s, where all of the available torque from the limiting actuator is used to compensate for velocity effects and gravity forces. Therefore, no worst-case accelerations \dot{v}_{u_2} and $\dot{\omega}_{u_2}$ can be obtained. However, accelerations can be obtained in directions other than worst-case acceleration directions. Fig. 7 shows the worst-case directions of translational velocity, denoted \hat{v}_{u_2} and $-\hat{v}_{u_2}$. The worst-case translational velocities of the end-effector operational point from this configuration, associated with point **C**, are expressed as

$$\begin{aligned} v_{u_2} &= \{ |v| \hat{v}_{u_2}, -|v| \hat{v}_{u_2} \} \\ &= \{ (0.34 \text{ m/s}) \hat{v}_{u_2}, -(0.34 \text{ m/s}) \hat{v}_{u_2} \}. \end{aligned} \quad (32)$$

An equal or higher level of translational velocity can be sustained in directions other than \hat{v}_{u_2} without saturating an actuator. These worst-case velocity directions remain the same for all combinations of acceleration and velocity described by the surface in Fig. 6. However, the magnitude of the worst-case velocity, $|v|$, decreases along the surface as the balanced accelerations increase. The worst-case translational velocity and acceleration directions, \hat{v}_{u_2} and $\hat{\omega}_{u_2}$, are nearly opposites as expected, but not exactly opposites, as shown by $-\hat{v}_{u_2}$.

The nonintercept regions of the dynamic capability surface in Fig. 6 show the achievable combinations of the worst-case accelerations and velocities, \dot{v}_{u_2} , $\dot{\omega}_{u_2}$, and v_{u_2} . The magnitudes of a particular combination of the worst-case accelerations and velocities represent a single point on the dynamic capability surface. In all directions other than the worst-case ones, higher accelerations are achievable and higher velocities are sustainable. Thus, the hypersurface describes the lower bound on the dynamic performance of the mechanism at a particular configuration.

This example allows the following general summary:

- combinations of acceleration, velocity, and force having magnitudes that *lie on or beneath* the dynamic capability hypersurface are achievable in and about every direction;
- combinations of acceleration, velocity, and force having magnitudes that *lie above* the dynamic capability hypersurface are not achievable in the worst-case, and possibly other, directions.

Since the dynamic capability hypersurface is difficult to display, measures are needed to summarize its characteristics. The $|v| = |\omega| = 0$ hypersurface section is convex, suggesting that the intercepts can be used to describe its size, denoted

$$\{ |\dot{v}|_x : |\dot{\omega}|_x : |f|_x : |m|_x : |v|_x : |\omega|_x \} \quad (33)$$

although it is difficult to draw conclusions about the shape of the hypersurface when velocities are included. The intercepts for the dynamic capability hypersurface of Fig. 6 are

$$\{ 7.9 \text{ m/s}^2 : 70 \text{ rad/s}^2 : 126 \text{ N} : 16 \text{ Nm} : 0.34 \text{ m/s} : 2.7 \text{ rad/s} \}.$$

VI. APPLICATIONS

The DCE have several uses in the analysis, design, and control of robotic manipulators. A short list of these include the following.

- 1) Comparing the suitability of different manipulators given the dynamic performance requirements of the task.
- 2) Characterizing the dynamic performance of a manipulator over its workspace or along a path by discretizing the region into a representative set of configurations, and statistically analyzing the DCE for the configurations in the set.
- 3) Motion planning which can use the worst-case direction information to avoid low performance configurations in a robot's workspace.
- 4) Selecting actuators for achieving a desired level of dynamic performance or actuator selection.

Extensive work has been done on the actuator-selection problem. The idea is to solve the inverse of the problem that was addressed in this paper, which was to determine the dynamic performance given the limits on actuator torque. In other words, given \mathbb{T} , find the balanced quantities. The actuator-selection problem involves finding the actuators that will provide a desired level of dynamic performance in and about every direction; given the balanced quantities, find \mathbb{T} , which determines the size of the actuators.

Optimization and heuristic procedures were developed for this problem in [28]. The balanced quantities are given in a number of performance points of a form similar to (33), which specify the desired shape of the dynamic capability hypersurface. Since the balanced velocities are specified, it is always possible to determine η in (24) for each performance point, so the developments discussed in Section V-D are useful for the actuator-selection method developed in [28].

VII. CONCLUSION

In this paper, the DCE were developed as a tool for analyzing the acceleration and force capabilities of nonredundant manipulators, including velocity effects, at a particular configuration for nonredundant manipulators with as many actuators as DOFs. This was accomplished while addressing unit inhomogeneities and unifying the analysis of acceleration, force, and velocity. These developments allowed for the analysis of any nonredundant mechanism with as many actuators as DOFs, as was illustrated by the analysis of the 6-DOF PUMA 560 robotic manipulator. In addition, the analysis also yielded insights into the limiting actuators, the motors which saturate attempting to produce end-effector motions and forces. The analysis also provided information about the worst-case acceleration, force, and velocity directions which saturate the limiting actuator(s).

APPENDIX I EQUATIONS OF MOTION

The joint space form of the equations of motion is

$$A(\mathbf{q}) \ddot{\mathbf{q}} + \mathbf{b}(\mathbf{q}, \dot{\mathbf{q}}) + \mathbf{g}(\mathbf{q}) + J^T \begin{bmatrix} \mathbf{f} \\ \mathbf{m} \end{bmatrix} = \mathbf{\Gamma} = \mathbf{G}^T \mathbf{\Upsilon} \quad (34)$$

where \mathbf{q} is the vector of generalized/joint coordinates, $A(\mathbf{q})$ is the inertia matrix, \mathbf{G} is the transmission matrix between joint and actuator torques, and $\mathbf{b}(\mathbf{q}, \dot{\mathbf{q}})$, $\mathbf{g}(\mathbf{q})$, $\mathbf{\Gamma}$, and $\mathbf{\Upsilon}$ are vectors of Coriolis/centrifugal, gravity, joint, and actuator forces.

The manipulator Jacobian J can be expressed as

$$\boldsymbol{\vartheta} \triangleq \begin{bmatrix} \mathbf{v} \\ \boldsymbol{\omega} \end{bmatrix} = J(\mathbf{q}) \dot{\mathbf{q}} \quad \mathbf{\Gamma} = J^T(\mathbf{q}) \mathbf{F} \quad (35)$$

where \mathbf{F} represents the actuator forces as perceived at the end-effector. Using (34) and (35), the actuator Jacobian J_a can be expressed as

$$\Upsilon = J_a^T \mathbf{F} = (J\mathbf{G}^{-1})^T \mathbf{F}. \quad (36)$$

Equations (34), (35), and (36) yield (1)

$$E \begin{bmatrix} \dot{\mathbf{v}} \\ \dot{\boldsymbol{\omega}} \end{bmatrix} + \varepsilon \begin{bmatrix} \mathbf{f} \\ \mathbf{m} \end{bmatrix} + \mathbf{C}(\mathbf{v}, \boldsymbol{\omega}) + \mathbf{g} = \Upsilon$$

where

$$\begin{aligned} E &= \mathbf{G}^{-T} A J^{-1} & \varepsilon &= J_a^T \\ \boldsymbol{\mu}(\mathbf{q}, \dot{\mathbf{q}}) &= \mathbf{G}^{-T} (\mathbf{b} - A J^{-1} \dot{\mathbf{J}} \dot{\mathbf{q}}) & \mathbf{g} &= \mathbf{G}^{-T} \mathbf{g} \\ \mathbf{C}(\mathbf{v}, \boldsymbol{\omega}) &= \boldsymbol{\mu} \left(\mathbf{q}, J^{-1} \begin{bmatrix} \mathbf{v}^T \\ \boldsymbol{\omega}^T \end{bmatrix} \right). \end{aligned} \quad (37)$$

APPENDIX II

SOLUTION FOR ACCELERATION AND FORCE TERMS

Here the optimization problem for the acceleration and force terms from Section V is addressed. However, only the acceleration terms from Section V-C, (19) will be discussed because the analysis of forces is identical

$$\begin{aligned} \max_{\dot{\mathbf{v}}, \dot{\boldsymbol{\omega}}} \quad \text{or} \quad \min_{\dot{\mathbf{v}}, \dot{\boldsymbol{\omega}}} \bar{\Upsilon}_i &:= \Upsilon_{\dot{\mathbf{v}}_i} + \Upsilon_{\dot{\boldsymbol{\omega}}_i} = E_{\mathbf{v}_i} \dot{\mathbf{v}} + E_{\boldsymbol{\omega}_i} \dot{\boldsymbol{\omega}} \\ \text{subject to } \dot{\mathbf{v}}^T \dot{\mathbf{v}} &= |\dot{\mathbf{v}}|^2 & \dot{\boldsymbol{\omega}}^T \dot{\boldsymbol{\omega}} &= |\dot{\boldsymbol{\omega}}|^2. \end{aligned}$$

In the Lagrange multiplier method, the critical points satisfy the constraints and the following equation:

$$\frac{\partial \bar{\Upsilon}_i}{\partial \dot{\vartheta}_j} = \lambda_1 \frac{\partial f}{\partial \dot{\vartheta}_j} + \lambda_2 \frac{\partial g}{\partial \dot{\vartheta}_j} \quad (38)$$

where $j = (1, \dots, n)$, λ_1 , and λ_2 are scalars, and

$$\begin{aligned} f &= \dot{\mathbf{v}}^T \dot{\mathbf{v}} - |\dot{\mathbf{v}}|^2 = 0 \\ g &= \dot{\boldsymbol{\omega}}^T \dot{\boldsymbol{\omega}} - |\dot{\boldsymbol{\omega}}|^2 = 0. \end{aligned} \quad (39)$$

Applying (38) to (19) yields

$$\begin{bmatrix} E_{\mathbf{v}_i}^T \\ E_{\boldsymbol{\omega}_i}^T \end{bmatrix} = \begin{bmatrix} 2\lambda_1 \mathbf{I} & 0 \\ 0 & 2\lambda_2 \mathbf{I} \end{bmatrix} \begin{bmatrix} \dot{\mathbf{v}} \\ \dot{\boldsymbol{\omega}} \end{bmatrix}. \quad (40)$$

Equation (40) can be expressed as

$$E_{\mathbf{v}_i}^T = 2\lambda_1 \dot{\mathbf{v}} \quad E_{\boldsymbol{\omega}_i}^T = 2\lambda_2 \dot{\boldsymbol{\omega}}. \quad (41)$$

Notice that the translational and rotational terms have decoupled. Equations (39) and (41) yield

$$\lambda_1^2 = \frac{E_{\mathbf{v}_i} E_{\mathbf{v}_i}^T}{4|\dot{\mathbf{v}}|^2} \quad \lambda_2^2 = \frac{E_{\boldsymbol{\omega}_i} E_{\boldsymbol{\omega}_i}^T}{4|\dot{\boldsymbol{\omega}}|^2}. \quad (42)$$

$(\bar{\Upsilon}_i)_{\max}$ and $(\bar{\Upsilon}_i)_{\min}$ are obtained using the positive and negative roots for λ_1 and λ_2 , which are substituted into (41) to obtain the solutions, or worst-case accelerations, $\dot{\mathbf{v}}_{ui}$, $\dot{\mathbf{v}}_{li}$, $\dot{\boldsymbol{\omega}}_{ui}$, and $\dot{\boldsymbol{\omega}}_{li}$ for the bounds on the i th actuator, expressed as

$$\begin{aligned} \dot{\mathbf{v}}_{ui} &= |\dot{\mathbf{v}}| \hat{\mathbf{v}}_{ui} = |\dot{\mathbf{v}}| \frac{E_{\mathbf{v}_i}^T}{\|E_{\mathbf{v}_i}\|} \\ \dot{\mathbf{v}}_{li} &= |\dot{\mathbf{v}}| \hat{\mathbf{v}}_{li} = |\dot{\mathbf{v}}| \frac{-E_{\mathbf{v}_i}^T}{\|E_{\mathbf{v}_i}\|} \\ \dot{\boldsymbol{\omega}}_{ui} &= |\dot{\boldsymbol{\omega}}| \hat{\boldsymbol{\omega}}_{ui} = |\dot{\boldsymbol{\omega}}| \frac{E_{\boldsymbol{\omega}_i}^T}{\|E_{\boldsymbol{\omega}_i}\|} \\ \dot{\boldsymbol{\omega}}_{li} &= |\dot{\boldsymbol{\omega}}| \hat{\boldsymbol{\omega}}_{li} = |\dot{\boldsymbol{\omega}}| \frac{-E_{\boldsymbol{\omega}_i}^T}{\|E_{\boldsymbol{\omega}_i}\|} \end{aligned} \quad (43)$$

where the subscripts “ u ” and “ l ” indicate the upper and lower bounds. The optimal values can be expressed as

$$\begin{aligned} (\bar{\Upsilon}_i)_{\max} &= E_{\mathbf{v}_i} \dot{\mathbf{v}}_{ui} + E_{\boldsymbol{\omega}_i} \dot{\boldsymbol{\omega}}_{ui} = \|E_{\mathbf{v}_i}\| |\dot{\mathbf{v}}| + \|E_{\boldsymbol{\omega}_i}\| |\dot{\boldsymbol{\omega}}| \\ (\bar{\Upsilon}_i)_{\min} &= E_{\mathbf{v}_i} \dot{\mathbf{v}}_{li} + E_{\boldsymbol{\omega}_i} \dot{\boldsymbol{\omega}}_{li} = -\|E_{\mathbf{v}_i}\| |\dot{\mathbf{v}}| - \|E_{\boldsymbol{\omega}_i}\| |\dot{\boldsymbol{\omega}}|. \end{aligned} \quad (44)$$

From here, the elements of \mathbf{A} in (28) are easy to discern. Similar expressions can be developed for \mathbf{F} in (28).

APPENDIX III

SOLUTION FOR VELOCITY TERMS

Here only the maximization problem is discussed, since it is so similar to the minimization. The velocity portion of the optimization problem given in (23) is

$$\begin{aligned} \max_{\mathbf{v}, \boldsymbol{\omega}} \Upsilon_{\bar{\mathbf{h}}_i} &:= \boldsymbol{\vartheta}^T \bar{\mathbf{H}}_i \boldsymbol{\vartheta} \\ \text{subject to } \mathbf{v}^T \mathbf{v} &= |\mathbf{v}|^2 & \boldsymbol{\omega}^T \boldsymbol{\omega} &= |\boldsymbol{\omega}|^2. \end{aligned} \quad (45)$$

Since \mathbf{v} and $\boldsymbol{\omega}$ lie on bounded, closed surfaces/curves, forming a compact set, the global maximum and minimum exist.

A. Special Case: Decoupled Subspaces

When $\bar{\mathbf{H}}_i$ is decoupled with respect to \mathbf{v} and $\boldsymbol{\omega}$

$$\bar{\mathbf{H}}_i = \begin{bmatrix} \bar{\mathbf{H}}_{i\mathbf{v}} & 0 \\ 0 & \bar{\mathbf{H}}_{i\boldsymbol{\omega}} \end{bmatrix} \quad (46)$$

the problem can be solved using the method of Lagrange multipliers, see Appendix II, resulting in an eigenvalue problem. The maximum value has the form

$$\begin{aligned} (\Upsilon_{\bar{\mathbf{h}}_i})_{\max} &= \mathbf{v}_{ui}^T \bar{\mathbf{H}}_{i\mathbf{v}} \mathbf{v}_{ui} + \boldsymbol{\omega}_{ui}^T \bar{\mathbf{H}}_{i\boldsymbol{\omega}} \boldsymbol{\omega}_{ui} \\ &= \varepsilon_{\mathbf{v}_i} |\mathbf{v}|^2 + \varepsilon_{\boldsymbol{\omega}_i} |\boldsymbol{\omega}|^2 \end{aligned} \quad (47)$$

where $\varepsilon_{\mathbf{v}_i}$ and $\varepsilon_{\boldsymbol{\omega}_i}$ are the largest eigenvalues of $\bar{\mathbf{H}}_{i\mathbf{v}}$ and $\bar{\mathbf{H}}_{i\boldsymbol{\omega}}$. The worst-case directions are the associated unit eigenvectors $\bar{\boldsymbol{\varepsilon}}_{\mathbf{v}_i}$ and $\bar{\boldsymbol{\varepsilon}}_{\boldsymbol{\omega}_i}$. The worst-case velocities are defined as

$$\begin{aligned} \mathbf{v}_{ui} &= \{|\mathbf{v}| \hat{\mathbf{v}}_{ui1}, -|\mathbf{v}| \hat{\mathbf{v}}_{ui1}\} \\ &= \{|\mathbf{v}| \bar{\boldsymbol{\varepsilon}}_{\mathbf{v}_i}, -|\mathbf{v}| \bar{\boldsymbol{\varepsilon}}_{\mathbf{v}_i}\} \\ \boldsymbol{\omega}_{ui} &= \{|\boldsymbol{\omega}| \hat{\boldsymbol{\omega}}_{ui1}, -|\boldsymbol{\omega}| \hat{\boldsymbol{\omega}}_{ui1}\} \\ &= \{|\boldsymbol{\omega}| \bar{\boldsymbol{\varepsilon}}_{\boldsymbol{\omega}_i}, -|\boldsymbol{\omega}| \bar{\boldsymbol{\varepsilon}}_{\boldsymbol{\omega}_i}\}. \end{aligned} \quad (48)$$

B. Special Case: $|\boldsymbol{\omega}| = \eta |\mathbf{v}|$

A change of variables using $|\boldsymbol{\omega}| = \eta |\mathbf{v}|$ to express \mathbf{v} and $\boldsymbol{\omega}$ in terms of the unit vectors $\bar{\mathbf{v}}$ and $\bar{\boldsymbol{\omega}}$

$$\begin{bmatrix} \mathbf{v} \\ \boldsymbol{\omega} \end{bmatrix} = |\mathbf{v}| \begin{bmatrix} \mathbf{I} & 0 \\ 0 & \eta \mathbf{I} \end{bmatrix} \begin{bmatrix} \bar{\mathbf{v}} \\ \bar{\boldsymbol{\omega}} \end{bmatrix} = |\mathbf{v}| \begin{bmatrix} \mathbf{I} & 0 \\ 0 & \eta \mathbf{I} \end{bmatrix} \bar{\boldsymbol{\vartheta}} \quad (49)$$

yields

$$\begin{aligned} \max_{\bar{\mathbf{v}}, \bar{\boldsymbol{\omega}}} \Upsilon_{\bar{\mathbf{h}}_i} &:= |\mathbf{v}|^2 \bar{\boldsymbol{\vartheta}}^T \bar{\mathbf{H}}_i(\eta) \bar{\boldsymbol{\vartheta}} \\ \text{subject to } \bar{\mathbf{v}}^T \bar{\mathbf{v}} &= 1 & \bar{\boldsymbol{\omega}}^T \bar{\boldsymbol{\omega}} &= 1 \end{aligned} \quad (50)$$

where

$$\Upsilon_{\bar{\mathbf{h}}_i} = |\mathbf{v}|^2 \begin{bmatrix} \bar{\mathbf{v}} \\ \bar{\boldsymbol{\omega}} \end{bmatrix}^T \begin{bmatrix} \bar{\mathbf{H}}_{i\mathbf{v}} & \eta \bar{\mathbf{H}}_{i\mathbf{v}\boldsymbol{\omega}} \\ \eta \bar{\mathbf{H}}_{i\boldsymbol{\omega}\mathbf{v}} & \eta^2 \bar{\mathbf{H}}_{i\boldsymbol{\omega}} \end{bmatrix} \begin{bmatrix} \bar{\mathbf{v}} \\ \bar{\boldsymbol{\omega}} \end{bmatrix}. \quad (51)$$

$\bar{H}_i(\eta)$ has homogeneous units, and $|v|$ is a constant multiplying the quadratic term, which can now be numerically maximized. Several initial guesses must be tried to insure the global maximum is found, since this problem is nonconvex. An alternative to this has been developed, which is guaranteed to find the global maximum using *dialytic elimination* in [29].

The solution $\bar{\varepsilon}_i$ obtained from either procedure yields

$$\begin{bmatrix} v_{ui} \\ \omega_{ui} \end{bmatrix} = \pm |v| \begin{bmatrix} \mathbf{I} & 0 \\ 0 & \eta \mathbf{I} \end{bmatrix} \bar{\varepsilon}_i. \quad (52)$$

The maximum value ε_i obtained from either procedure yields

$$(\Upsilon_{\bar{H}_i})_{\max} = \varepsilon_i |v|^2. \quad (53)$$

ACKNOWLEDGMENT

The authors would like to thank Prof. B. Roth from the Mechanical Engineering Department at Stanford University for advice concerning the invariance issues discussed here. Also thanks to Dr. M. Van der Loos of the Palo Alto VA Rehabilitation R&D Center and Dr. C. H. Kim for their help in the preparation of this paper.

REFERENCES

- [1] H. Lipkin and J. Duffy, "Hybrid twist and wrench control for a robotic manipulator," *J. Mechanisms, Transmissions, Autom. Des.*, vol. 110, pp. 138–144, Jun. 1988.
- [2] J. Duffy, "Editorial: The fallacy of modern hybrid control theory that is based on "orthogonal complements" of twist and wrench spaces," *J. Robot. Syst.*, vol. 7, no. 2, pp. 139–144, 1990.
- [3] K. Kazerounian and J. Rastegar, "Object norms: A class of coordinate and metric independent norms for displacements," *Flexible Mechanisms, Dynam., Anal.*, vol. 47, pp. 271–275, 1992.
- [4] K. L. Doty, C. Melchiorri, E. M. Schwartz, and C. Bonivento, "Robot manipulability," *IEEE Trans. Robot. Autom.*, vol. 11, pp. 462–468, Jun. 1995.
- [5] J. L. Jones and A. M. Flynn, *Mobile Robots: Inspiration to Implementation*. Natick, MA: A. K. Peters, 1993, pp. 170–176.
- [6] J. Vertut and A. Liegeois, "General design criteria for manipulators," *Mech. Mach. Theory*, vol. 16, no. 1, pp. 65–70, 1981.
- [7] O. Khatib, "Inertial properties in robotic manipulation: An object-level framework," *Int. J. Robot. Res.*, vol. 13, no. 1, pp. 19–36, Feb. 1995.
- [8] H. Asada, "A geometrical representation of manipulator dynamics and its application to arm design," *J. Dynam. Syst., Meas., Control*, vol. 105, no. 3, pp. 131–135, Sep. 1983.
- [9] O. Ma and J. Angeles, "The concept of dynamic isotropy and its applications to inverse kinematics and trajectory planning," in *Proc. IEEE Int. Conf. Robot. Autom.*, vol. 1, 1990, pp. 481–486.
- [10] J. R. Singh and J. Rastegar, "Optimal synthesis of robot manipulators based on global dynamic parameters," *Int. J. Robot. Res.*, vol. 11, no. 6, pp. 538–548, 1992.
- [11] O. Khatib and J. Burdick, "Optimization of dynamics in manipulator design: The operational space formulation," *Int. J. Robot. Autom.*, vol. 2, no. 2, pp. 90–98, 1987.
- [12] T. Yoshikawa, "Dynamic manipulability of robot manipulators," in *Proc. IEEE Int. Conf. Robot. Autom.*, St. Louis, MO, 1985, pp. 1033–1038.
- [13] P. Chiacchio, S. Chiaverini, L. Sciavicco, and B. Siciliano, "Reformulation of dynamic manipulability ellipsoid for robotic manipulators," in *Proc. IEEE Int. Conf. Robot. Autom.*, vol. 3, Sacramento, CA, 1991, pp. 2192–2197.
- [14] T. J. Graettinger and B. H. Krogh, "The acceleration radius: A global performance measure for robotic manipulators," *IEEE J. Robot. Autom.*, vol. 4, pp. 60–69, Feb. 1988.
- [15] Y. Kim and S. Desa, "The definition, determination, and characterization of acceleration sets for spatial manipulators," *Int. J. Robot. Res.*, vol. 12, no. 6, pp. 572–587, 1993.
- [16] T. Yoshikawa, "Manipulability of robotic mechanisms," *Int. J. Robot. Res.*, vol. 4, no. 2, pp. 3–9, 1985.
- [17] J. Lee, "A structured algorithm for minimum l_∞ -norm solutions and its application to a robot velocity workspace analysis," *Robotica*, vol. 19, pp. 343–352, 2001.
- [18] P. Chiacchio and Y. Bouffard-Vercelli, "Force polytope and force ellipsoid for redundant manipulators," *J. Robot. Syst.*, vol. 14, no. 8, pp. 613–620, 1997.
- [19] J. K. Salisbury and J. J. Craig, "Articulated hands: Force control and kinematic issues," *Int. J. Robot. Res.*, vol. 1, no. 1, pp. 4–17, 1982.
- [20] C. Gosselin, "Dexterity indices for planar and spherical robotic manipulators," in *Proc. IEEE Int. Conf. Robot. Autom.*, 1990, pp. 650–655.
- [21] J. Angeles and C. S. López-Cajún, "Kinematic isotropy and the conditioning index of serial robotic manipulators," *Int. J. Robot. Res.*, vol. 11, no. 6, pp. 560–571, Dec. 1992.
- [22] F. C. Park and R. W. Brockett, "Kinematic dexterity of robot mechanisms," *Int. J. Robot. Res.*, vol. 13, no. 1, pp. 1–15, 1994.
- [23] T. Yoshikawa, "Translational and rotational manipulability of robotic manipulators," in *Proc. Int. Conf. Ind. Electron., Control, Instrum.*, Oct. 1991, pp. 1170–1175.
- [24] J. Lee, "A study on the manipulability measures for robot manipulators," in *Proc. IEEE/RSJ Int. Conf. Intell. Robots, Syst.*, 1997, pp. 1458–1465.
- [25] A. Bowling and O. Khatib, "Design of macro/mini manipulators for optimal dynamic performance," in *Proc. IEEE Int. Conf. Robot. Autom.*, vol. 1, Albuquerque, NM, Apr. 1997, pp. 449–454.
- [26] J. S. Arora, *Introduction to Optimum Design*. New York: McGraw-Hill, 1989.
- [27] B. Armstrong, O. Khatib, and J. Burdick, "The explicit model and inertial parameters of the PUMA 560 arm," in *Proc. IEEE Int. Conf. Robot. Autom.*, vol. 1, 1986, pp. 510–518.
- [28] A. Bowling and O. Khatib, "The dynamic loading criteria in actuator selection for desired dynamic performance," *Adv. Robot.*, vol. 17, no. 7, pp. 641–656, Nov. 2003.
- [29] C. Kim and A. Bowling, "End-effector velocity effects on robotic manipulator dynamic performance: An analytical approach," in *Proc. IEEE/RSJ Int. Conf. Intell. Robots, Syst.*, vol. 2, Coimbra, Portugal, Jun. 2003, pp. 770–775.